Drug Design, Development and Therapy

Dovepress
Taylor & Francis Group

Open Access Full Text Article

ORIGINAL RESEARCH

Ciprofol Alleviates Depressive-Like Behaviors in CUMS Mice Through PPARα-Associated ERK/CREB Signaling Activation

Jiaqi Li[1,2,*], Meiqin Chen[3–5,*], Yuan Lin[5], Qian Wu[5], Jiahong Shen[2], Yuxin Wen[6], Siyue Li[1], Jie Zhang[3–5], Jianliang Sun[1,2]

[1]Zhejiang University School of Medicine, Hangzhou, People's Republic of China; [2]Department of Anesthesiology, Affiliated Hangzhou First People's Hospital, School of Medicine, Westlake University, Hangzhou, People's Republic of China; [3]Department of Neurology, Sichuan Provincial People's Hospital, School of Medicine, University of Electronic Science and Technology of China, Chengdu, People's Republic of China; [4]The Key Laboratory of Neural and Vascular Biology, Ministry of Education, College of Basic Medicine, Hebei Medical University, Shijiazhuang, People's Republic of China; [5]Institute of Neuroscience, College of Medicine, Xiamen University, Xiamen, People's Republic of China; [6]Department of Anesthesiology, The Second Affiliated Hospital of Zhejiang University, Hangzhou, People's Republic of China

*These authors contributed equally to this work

Correspondence: Jianliang Sun; Jie Zhang, Email jxmzsjl@163.com; jiezhang@xmu.edu.cn

Background: Depression is a complex neuropsychiatric disorder involving neuroinflammation, synaptic dysfunction, and neurotransmitter dysregulation. Recent studies have highlighted the therapeutic potential of short-acting anesthetics in the treatment of depression. Ciprofol, a novel intravenous anesthetic with rapid onset and recovery, shows promise, although its antidepressant mechanisms remain underexplored.

Methods: We induced a depressive-like phenotype in mice using a 5-week chronic unpredictable mild stress (CUMS) protocol. Following model establishment, the mice received intraperitoneal injections of ciprofol (25 mg/kg) for 7 days. Behavioral assessments included the sucrose preference test (SPT), tail suspension test (TST), and forced swimming test (FST). To investigate neuroinflammation and microglial activation in the prefrontal cortex (PFC), we employed immunofluorescence staining, three-dimensional reconstruction, and quantitative real-time PCR (qRT-PCR). Synaptic structural changes were assessed using Western blot, three-dimensional reconstruction, and Golgi staining. Furthermore, transcriptome sequencing and Western blot were performed to elucidate the potential mechanisms underlying the antidepressant effects of ciprofol.

Results: Ciprofol treatment alleviated CUMS-induced depressive behaviors, as evidenced by reduced immobility time and increased sucrose preference. Ciprofol suppressed PFC microglial activation and downregulated pro-inflammatory cytokines, while preserving synaptic integrity by inhibiting microglia-mediated synaptic phagocytosis. Mechanistic studies suggested that ciprofol's antidepressant effect might be mediated by PPARα activation, which potentially triggers the ERK/CREB pathway, as indicated by transcriptome analysis and Western blot.

Conclusion: Ciprofol can alleviate the depressive-like behaviors in CUMS mice by inhibiting the inflammatory response and reducing synaptic loss, and the mechanism may be related to the activation of the PPARα-mediated ERK/CREB pathway.

Keywords: depression, ciprofol, microglia, neuroinflammation, peroxisome proliferator-activated receptor α

Introduction

Depression is a debilitating mental disorder affecting approximately 264 million people worldwide, with core symptoms including persistent low mood, anhedonia, and cognitive impairment.[1] Extensive research has revealed that the pathogenesis of depression is multifactorial, encompassing genetic predispositions, early-life traumatic experiences (eg, abuse and neglect), chronic stress, and comorbid somatic illnesses.[2] In the clinical management of major depressive disorder (MDD), selective serotonin reuptake inhibitors (SSRIs) are predominantly employed as first-line antidepressants.[3,4] However, nearly 30–40% of patients show treatment resistance.[5] In addition, prolonged SSRI use is associated with

Received: 7 April 2025
Accepted: 23 August 2025
Published: 30 August 2025

a substantial increase in adverse events, including but not limited to sexual dysfunction,[6] emotional blunting,[7] weight gain,[8] gastrointestinal disturbances,[9] and withdrawal symptoms upon discontinuation.[10] Additionally, rare but serious risks such as QT prolongation (with certain SSRIs)[11] and increased bleeding tendency have been reported in long-term users.[12] These clinical challenges highlight the critical need for novel therapeutic approaches.

The emergence of rapid-acting anesthetics as antidepressants has revolutionized depression treatment, particularly for treatment-resistant depression (TRD).[13] Following ketamine's success, propofol has shown promising antidepressant properties through dopamine transporter modulation[14] and astrocyte protection,[15] with clinical effects comparable to ECT but better tolerated.[16] Given these neuroprotective and potentially antidepressant attributes of propofol, it is hypothesized that its structural analog, ciprofol, might exhibit comparable antidepressant effects.

Ciprofol, a 2,6-disubstituted phenol derivative structurally related to propofol,[17] demonstrates enhanced $GABA_A$ receptor affinity (4-5-fold greater than propofol) due to its cyclopropyl modification.[18] This novel intravenous anesthetic retains propofol's favorable pharmacokinetics (rapid onset/recovery),[19] while showing improved safety profiles, including reduced injection pain and cardiorespiratory depression.[20] These properties make ciprofol an attractive candidate for clinical sedation. Previous studies have confirmed that ciprofol has significant neuroprotective effects[21] and anti-inflammatory properties,[22] although its antidepressant effects and underlying mechanisms have not been thoroughly investigated. This study systematically evaluates ciprofol's antidepressant potential and underlying mechanisms to expand therapeutic options for depression.

The prefrontal cortex (PFC) plays a critical role in the generation and regulation of emotion[23] and its dysfunction is linked to stress-related disorders like MDD.[24] Neuroimaging studies have revealed significantly elevated levels of 18-kDa translocator protein (TSPO) in the PFC of MDD patients, indicating microglial activation.[25,26] As resident immune cells of the central nervous system, microglia serve as pivotal regulators of neuroinflammatory processes.[27] Activated microglia can exacerbate neuroinflammation through excessive release of proinflammatory cytokines (eg, IL-1β, TNF-α, and IL-6).[28] Notably, preclinical studies demonstrate that pharmacological normalization of IL-1β levels in the PFC significantly ameliorates lipopolysaccharide (LPS)-induced anxiety and depressive-like behaviors in mice.[29,30]

One of the key pathophysiological features of MDD involves the impairment of excitatory synapses in the PFC.[31] Emerging evidence suggests that in adolescents with depression, microglia-mediated chronic neuroinflammation may activate specific cellular signaling cascades and contribute to central synaptic loss.[32] Moreover, hyperactivated microglia can exacerbate synaptic damage through complement-dependent synaptic pruning mechanisms.[33] Importantly, preclinical studies demonstrate that the SSRI (escitalopram) effectively reverses synaptic deficits in the CUMS mouse model.[34]

In this study, we combined transcriptomic and neurobiological analyses to uncover novel molecular targets underlying ciprofol's potential antidepressant effects. Using a CUMS mouse model, we found that ciprofol alleviated depressive-like behaviors while reducing neuroinflammation and synaptic deficits. Mechanistic investigations revealed PPARα as a critical mediator of ciprofol's actions, suggesting its repurposing potential for psychiatric disorders beyond anesthesia.

Materials and Methods

Animals

Experimental Design for Mice

Mice were procured from the Xiamen Laboratory Animal Center, a certified Specific Pathogen Free (SPF) facility. The animals were housed in standard cages (five per cage) under controlled environmental conditions with a temperature of 22 ± 2°C and a 12-h light/dark cycle, with ad libitum access to food and water except during specific modeling and behavioral testing procedures. Prior to experimental manipulations, all mice were allowed a 7-day acclimation period to adapt to the housing conditions. All experimental protocols were approved by the Xiamen University Animal Ethics Committee (License No. XMULAC20190144 and XMULAC20240226) and conducted in strict compliance with China's national standard GB/T 35892–2018 (Guidelines for Ethical Review of Laboratory Animal Welfare) as well as the ARRIVE guidelines. In vitro cell experiments followed Good Cell Culture Practice (GCCP) guidelines.

We used 54 C57BL/6 male mice (7 weeks), weighing 19–22 g. Mice were randomly assigned to three groups (n=18 per group): (1) Control group: No treatment was administered; (2) CUMS group: Mice were subjected to CUMS for 5 weeks, followed by intraperitoneal injections of an equal volume of medium/long-chain fat emulsion

(Fresenius Kabi SSPC, Jiangsu, China) as a single dose or for 7 consecutive days; (3) CUMS + Ciprofol group: Mice were subjected to CUMS for 5 weeks, followed by intraperitoneal injections of Ciprofol (25 mg/kg, Liaoning Haisco Pharmaceutical Co., Ltd, Liaoning, China) as a single dose or for 7 consecutive days. Behavioral tests were conducted over 3 days, after which samples were collected. The experimental workflow is illustrated in Figure 1A.

Preparation of Depressive Model Mice

The CUMS procedure has undergone modifications in accordance with the provided description.[35,36] Depressive model mice were exposed to CUMS for 5 consecutive weeks. Two different stressors were randomly chosen each day, with the constraint that no single stressor was repeated on back-to-back days. The stressors included (1) 24 h of food deprivation; (2) 24 h of water deprivation; (3) 5 min in a 45°C incubator; (4) 6 h of social crowding stress; (5) 45-degree cage tilting; (6) 15 min of shaking; (7) 6 h of centrifuge tube restraint; (8) exposure to a noisy environment; (9) delayed lights off; (10) novel object: a centrifuge tube wrapped with yellow tape; and (11) damp bedding: mixing 200 mL of water evenly into every 100 g of bedding.

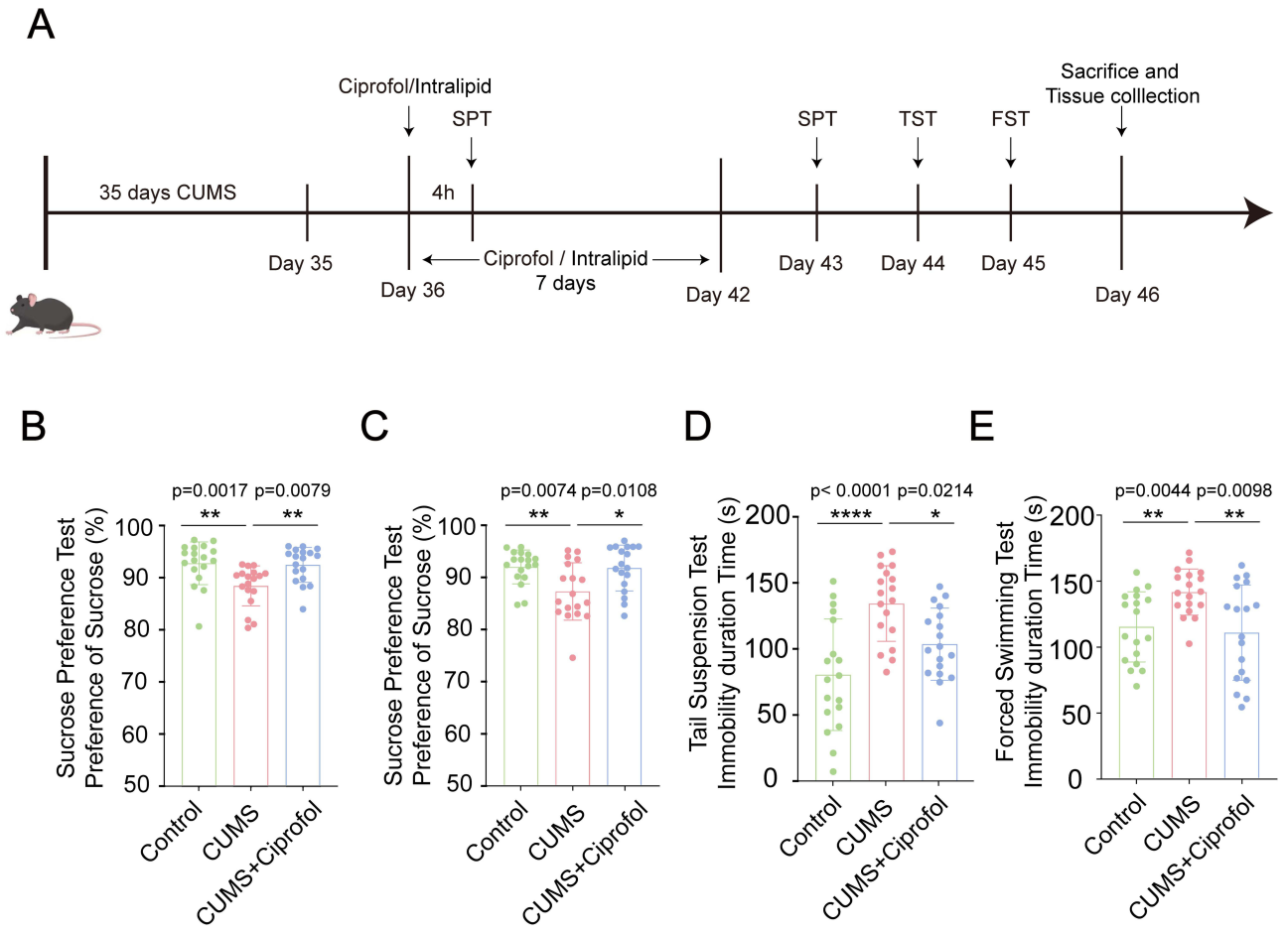

Figure 1 Ciprofol alleviates CUMS-induced depressive-like behaviors in mice. (**A**) A schematic diagram of the animal experimental procedure. (**B**) Quantification of sucrose preference in the sucrose preference test (SPT) of the Control group, CUMS group and CUMS + Ciprofol group at 4 h after a single intraperitoneal injection. (n = 18 per group, Kruskal–Wallis test followed by Dunn's post hoc test) (**C**) Quantification of sucrose preference in SPT of the Control group, CUMS group and CUMS + Ciprofol group after intraperitoneal injection for 7 days. (n = 18 per group, one-way ANOVA followed by Tukey's post hoc test) (**D**) Quantification of the immobility time in the tail suspension test (TST) of the Control group, CUMS group and CUMS + Ciprofol group. (n = 18 per group, one-way ANOVA followed by Tukey's post hoc test) (**E**) Quantification of the immobility time in the forced swimming test (FST) of the Control group, CUMS group and CUMS + Ciprofol group. (n = 18 per group, Welch's ANOVA followed by Games-Howell post hoc test). All data are expressed as mean ± SD. *p < 0.05, **p < 0.01, ****p < 0.0001.

Abbreviation: CUMS, chronic unpredictable mild stress.

https://doi.org/10.2147/DDDT.S532905

Behavioral Studies

Sucrose Preference Test (SPT)

The SPT was performed as previously described, with a slight modification.[37] Briefly, mice were housed individually in cages and trained to drink from two identical bottles. Forty-eight hours prior to the experiment, mice were trained to simultaneously drink 1% sucrose solution and regular water from the two bottles. Each bottle contained 55 ± 1g of liquid (either 1% sucrose solution or regular water). During this period, mice had unrestricted access to both liquids and food. To avoid positional bias, the positions of the containers were switched every 12 h. Twenty-four hours before the experiment, mice were subjected to food and water deprivation. On the day of the experiment, mice were given access to both bottles (1% sucrose solution and regular water) for 24 h. The initial weight of each liquid was recorded, and the weight remaining in each bottle was measured after 24 h. The sucrose preference was calculated using the following formula: Sucrose preference (%) = [Sucrose intake / (Sucrose + Water intake)] × 100%. This test was performed at the end of CUMS procedure, after a single dose of ciprofol, and after seven doses of ciprofol to assess the effects of chronic stress and subsequent drug treatment on sucrose preference.

Tail Suspension Test (TST)

The TST was performed as previously described, with a slight modification.[38] All animals were habituated to the testing room for 1 h before TST. TST was conducted using a 20×20×30 cm plastic chamber. During the experiment, mice were suspended by their tails from the apparatus for a duration of 6 minutes. The behavior of the mice was recorded and analyzed in real-time using a video tracking system (Smart 3.0). The immobility time of the mice during the last 4 minutes of the experiment was calculated to assess their activity related to escape behavior.

Forced Swimming Test (FST)

The FST was performed as previously described, with a slight modification.[39] All animals were habituated to the testing room for 1 h before FST. In the experiment, water maintained at a temperature of 25±1°C was filled in a transparent cylindrical container (diameter: 15 cm, height: 25 cm) to a depth of 15 cm. During the experiment, mice were submerged in the water for 6 min, and their behavior was recorded throughout using a video monitoring system (Smart 3.0). For data analysis, the immobility time of the mice in the last 4 min of the experiment was calculated to evaluate the escape-related behavior of the mice.

BV-2 Cell Culture Procedures

BV-2 cells (Shanghai CAS Cell Bank, Shanghai, China) were cultured in high-glucose DMEM supplemented with 10% FBS and 1% penicillin/streptomycin. The cells were maintained in a humidified incubator at 37°C with 5% CO_2, and the medium was changed every 2–3 days. For the experiments, cells were first stimulated with 0.1μg/mL LPS for 6 h, followed by treatment with various concentrations of ciprofol (50, 75, and 100μM) for an additional 6 h. The cells were randomly assigned to three groups: (1) Control group: cultured in serum medium without LPS and ciprofol; (2) LPS group: cultured in serum medium containing 0.1μg/mL LPS; and (3) LPS + ciprofol group: cultured in serum medium containing 0.1μg/mL LPS and different concentrations of ciprofol.

Protein Extraction and Western Blot

Prefrontal cortical tissues were dissected using anatomical landmarks and homogenized in ice-cold RIPA buffer (supplemented with protease/phosphatase inhibitors) at a 10:1 buffer-to-tissue ratio (μL:mg). Following homogenization with a grinder, the lysate was placed on ice and vortexed every 10 min for a total of three times to ensure complete lysis. The lysates were then centrifuged (12,000 rpm, 15 min, 4°C). The supernatant was mixed with 5× loading buffer (4:1 ratio), denatured at 100°C for 5 min, and stored at −80°C. Proteins were separated by SDS-PAGE and transferred to a membrane using the wet transfer method. The membranes were blocked with Tris-buffered saline and Tween (TBST) containing 5% nonfat milk/BSA and 0.1% Tween 20 for 2 h at room temperature and then incubated with primary antibodies overnight at 4°C. The following primary antibodies were used: rabbit anti-vGLUT2 (1:3000, CST, 12937S), mouse anti-PSD95 (1:3000, Thermo Fisher, MA1-045), rabbit anti-ERK1/2 (1:1000, CST, 5013S), rabbit anti-p-ERK1/2

(1:1000, CST, 4370S), rabbit anti-CREB (1:1000, CST, 9197T), rabbit anti-p-CREB (1:1000, CST, 9198S), rabbit anti-PPARα (1:1000, ABclonal, A25296) and mouse anti-GAPDH (1:10000, Proteintech, 60004-1-1g). The following day, the membrane was washed three times with TBST and incubated with horseradish peroxidase (HRP)-conjugated secondary antibodies for 1 hour. The secondary antibodies used were goat anti-mouse/rabbit antibodies, which were purchased from Millipore (AP132P, AP124P). Subsequently, chemiluminescent substrate was evenly applied to the surface of the PVDF membrane, which was then placed in a chemiluminescence imager for exposure. The bands were detected via an e-BLOT Touch Imager (Shanghai) and analyzed using ImageJ. Densitometric values of the proteins were normalized to GAPDH.

Immunofluorescence

Brain sections were first blocked and permeabilized with a mixture of 3% BSA and 0.3% Triton X-100 for 1 h, followed by washing with PBS. Subsequently, the sections were incubated overnight at 4°C on a horizontal shaker. After incubation, the sections were brought to room temperature for 4–5 h. The following primary antibodies were used: mouse anti-NeuN (1:400, Abcam, Ab104224), rabbit anti-Iba1 (1:400, CST, E404W), rabbit anti-S100β (1:400, Abcam, Ab52642), rabbit anti-vGLUT2 (1:200, CST, 12937s), mouse anti-PSD95 (1:400, Invitrogen, MA1-045). Secondary antibodies, selected based on the species of the primary antibodies, were diluted at 1:500. The sections were then incubated for 1 h at room temperature in the dark on a horizontal shaker. After secondary antibody incubation, the sections were washed with PBS. The sections were gently mounted in order onto prelabeled slides. Excess liquid was removed, and a mounting medium containing DAPI (1:1000, SIGMA, D8417) was applied, followed by slow cover-slip application to avoid bubble formation. Imaging was performed at appropriate magnifications based on experimental requirements. The laser wavelengths used were as follows: DAPI (405 nm), Alexa Fluor 488 (488 nm), and Alexa Fluor 594 (594 nm).

Three-Dimensional Reconstruction Technology

The three-dimensional reconstruction was performed as previously described.[40,41] Cortical sections were imaged with a confocal microscope (Nikon, A1R) equipped with a 60× oil-immersion objective, acquiring z-stack images at 0.5 μm intervals. To analyze both the volume of microglia and their synaptic engulfment activity, we performed immunostaining for microglia marker Iba1/CD68 and double immunostaining for the synaptic marker vGlut2/PSD95 with microglia (marker Iba1). Three-dimensional image rendering was conducted via Imaris software (v10.0.0, Bitplane, Switzerland). Briefly, microglial cells and vGlut2/PSD95-positive synapses were reconstructed using the surface rendering function, and the number of vGlut2/PSD95 puncta colocalized within Iba1-positive volumes was quantified. The engulfment index was calculated as the number of internalized vGlut2/PSD95 puncta divided by the microglial volume (μm^3). For each prefrontal cortical sample, a minimum of three non-overlapping fields were analyzed to ensure representative sampling.

Golgi-Cox Staining

Golgi staining was performed using a GenMED Golgi Stain Kit according to the manufacturer's protocol. Fresh brain samples were immediately immersed in a 1:1 mixture of solutions A and B and stored in complete darkness at room temperature for 14 days. Subsequently, the samples were transferred to 30% sucrose solution for 48 h in the dark, and 100 μm sections were obtained using a vibratome. The sections were mounted onto slides and air-dried for 24 h in the dark. After drying, the slides were rinsed three times with solution G (3 min per wash) and then incubated in solution H for 30 min. Following rinsing, the slides were immersed in a 1:1 mixture of solutions I and J for 20 min. Subsequently, the slides were dehydrated through a graded ethanol series and mounted on coverslips using Permount. For analysis, the slides were examined under a light microscope with a 100× oil-immersion objective (Olympus, FV1000). Only neurons in the PFC that were well-impregnated and clearly distinguishable from adjacent neurons were analyzed, and dendritic spine density was quantified using ImageJ.

Quantitative Real-Time PCR (qRT–PCR)

Quantitative real-time PCR was performed as described previously.[39] Total RNA was extracted with TRIzol™ Reagent (Invitrogen) and quantified using a NanoDrop™ OneC (Thermo Fisher). A total of 1000 ng of RNA was used for reverse transcription to synthesize cDNA. The RT reaction was performed at 37 °C for 15 min, 50 °C for 5 min, 98 °C for 5 min,

and 4 °C using a High-Capacity cDNA Reverse Transcription Kit with RNase Inhibitor (Toyobo, FSQ-201). qRT-PCR was then performed using the Step OnePlus^{TM} Real-Time PCR System (Thermo Fisher Scientific). The 10 μL reaction mix was composed of 5 μL of SYBR^{TM} Green Master Mix (Yeasen), 1 μL of each primer, 2 μL of cDNA and 1 μL of ddH_2O. All reactions were run on a Light Cycler 480 Instrument II (Roche Diagnostics, Basel, Switzerland) with a 15-min hot start at 95 °C followed by 40 cycles of 3-step thermocycling program: denaturation at 94 °C for 15s; annealing at 55 °C for 30s; and extension at 70 °C for 30s. Each sample was repeated twice. The fluorescent signals were collected during the extension stage, Ct values of the sample were calculated and data were analyzed using the $2^{-\Delta\Delta CT}$ method. The quantification data are presented as a ratio to the control level and β-actin was used as an internal reference. All primers were obtained by PrimerBank. Primers are shown in Table 1.

RNA Sequencing (RNA-Seq)

Total RNA was extracted using TRIzol reagent (Life Technologies). Subsequently, the quality of the RNA was assessed through multiple methods, including agarose gel electrophoresis, Nanodrop microspectrophotometer detection, and Agilent 2100 bioanalyzer detection. Following the confirmation of RNA integrity and purity, transcriptome library construction was carried out using the Hieff NGS® Ultima Dual-mode mRNA Library Prep Kit (Catalog No. 12309ES, Yeasen), strictly adhering to the manufacturer's instructions. For library quality inspection, the DNA 1000 assay Kit (Agilent Technologies, Catalog No. 5067–1504) or the High Sensitivity DNA assay Kit (Agilent Technologies, Catalog No. 5067–4626) was employed to ensure the library met the required standards. Finally, the RNA library sequencing was performed on the Illumina NovaSeq X Plus platform by Gene Denovo Biotechnology Co., Ltd. (Guangzhou, China).

Bioinformatic analysis was performed using Omicsmart, a dynamic real-time interactive online platform for data analysis (http://www.omicsmart.com). Differential expression analysis was carried out using the "edgeR" R package, and a p value <0.05 and |fold change| >1.3 were considered to indicate statistical significance. Visualization of the results was accomplished using the "ggplot2" R package to generate both volcano plots and heatmaps. Gene Ontology (GO) (http://geneontology.org) and Kyoto Encyclopedia of Genes and Genomes (KEGG) (http://www.genome.ad.jp/kegg/) functional and pathway enrichment analyses were performed. Correction for multiple testing was performed using the false discovery rate (FDR), with a threshold of FDR ≤ 0.05. Gene set enrichment analysis (GSEA) was conducted using default parameters in GSEA software, with enrichment scores and p values calculated accordingly.

Statistical Analysis

All the results are presented as the mean ± SD. The Shapiro–Wilk test was used to evaluate normality. The *F*-test and Brown-Forsythe test were used to verify the homogeneity of variance. For normally distributed data, an unpaired *t* test was used between two groups, and one-way ANOVA was used among multiple groups, followed by Tukey's post hoc test. If the variances were not equal, a *t* test with Welch's correction was used for comparisons between two groups, and

Table 1 The Primer Sequences Used for qRT-PCR

Gene	Species		Sequence (5'-3')
IL-6	Mouse	Forward	CCAAGAGGTGAGTGCTTCCC
		Reverse	CTGTTGTTCAGACTCTCTCCCT
IL-1β	Mouse	Forward	GCAACTGTTCCTGAACTCAACT
		Reverse	ATCTTTTGGGGTCCGTCAACT
TNF-α	Mouse	Forward	CCCTCACACTCAGATCATCTTCT
		Reverse	GCTACGACGTGGGCTACAG
iNOS	Mouse	Forward	GGAGTGACGGCAAACATGACT
		Reverse	TCGATGCACAACTGGGTGAAC
PPARα	Mouse	Forward	AGAGCCCCATCTGTCCTCTC
		Reverse	ACTGGTAGTCTGCAAAACCAAA
β-actin	Mouse	Forward	AAGTCCCTCACCCTCCCAAAAG
		Reverse	AAGCAATGCTGTCACCTTCCC

Welch ANOVA was used for comparisons among multiple groups, followed by Games–Howell post hoc test. Data that were not normally distributed were compared via the Mann–Whitney *U*-test or the Kruskal–Wallis test followed by Dunn's post hoc test. GraphPad Prism statistical software 10.0 was used to draw statistical maps. $P < 0.05$ was considered statistically significant.

Results

Ciprofol Ameliorates Depressive-Like Behaviors in CUMS Model Mice

To further explore the potential therapeutic effect of ciprofol on depression, male C57BL/6 mice were utilized to establish a depression model via the CUMS method for 5 weeks. Depressive-like behaviors in the mice were assessed via the SPT, TST, and FST. The behavioral results indicated that the CUMS model group exhibited significant depressive-like behaviors. In the SPT, CUMS-treated mice presented a marked reduction in sucrose preference (p=0.0286, Figure S1A), indicative of enhanced anhedonic behavior. In both the TST (p=0.0329, Figure S1B) and the FST (p=0.0109, Figure S1C), CUMS-treated mice had significantly prolonged immobility times, suggesting increased desperation behavior. These behavioral alterations were highly consistent with the core symptoms of depression, confirming that the CUMS approach successfully induced depressive-like behaviors in mice.

Three independent cohorts of animal experiments were designed for this study, with the experimental timelines depicted in Figure 1A. The results demonstrated that ciprofol significantly ameliorated depressive-like behaviors in CUMS model mice under both single-dose and continuous administration conditions. Initially, in the single-dose experiment, sucrose preference in CUMS model mice was significantly elevated 4 h after intraperitoneal injection of ciprofol (p= 0.0079, Figure 1B), indicating rapid alleviation of anhedonic behavior. Further investigation revealed that after 7 consecutive days of intraperitoneal ciprofol administration, sucrose preference in CUMS model mice was consistently and significantly increased (p= 0.0108, Figure 1C). In the TST (Figure 1D), the immobility time of the CUMS group (132.7 ± 28.37 s) was significantly longer than that of the control group (79.3 ± 41.88 s, $p < 0.0001$). However, the immobility time of the CUMS+Ciprofol group (102.2 ± 27.07 s) was shorter than that of the CUMS group ($p = 0.0214$). Similarly, the same trend was observed in the FST (Figure 1E). Specifically, the immobility times of mice in the control group, CUMS group and CUMS+Ciprofol group were 114.8 ± 26.69 s, 141.2 ± 17.55 s and 110.4 ± 36.23 s, respectively. These results indicate that ciprofol effectively improved anhedonic behavior and significantly reduced helplessness behavior.

Ciprofol Inhibits Neuroinflammation in CUMS Model Mice

To investigate the regulatory effect of ciprofol on neuroinflammation in CUMS model mice, immunofluorescence staining was used to analyze the expression levels of the glial cell surface markers Iba1 and S100β in the PFC of CUMS model mice after ciprofol treatment. The results showed that, compared with the control group (120.4 ± 29.65 cells/mm², $p = 0.0002$), the number of Iba1-labeled microglia in the PFC of the CUMS group was significantly increased by approximately 60.5% (193.2 ± 23.71 cells/mm²), indicating that CUMS induced microglial activation. However, CUMS-induced microglial activation was significantly reduced by approximately 25.2% after treatment with ciprofol (144.6 ± 11.97 cells/mm², $p = 0.0062$), suggesting that ciprofol effectively inhibited microglial overactivation and attenuated neuroinflammatory responses (Figure 2A and B). Further evaluation of astrocyte activation status revealed that the density of S100β-labeled astrocytes in the PFC of CUMS model mice was significantly increased (138.8 ± 32.77 cells/mm², $p = 0.02$). In contrast, ciprofol treatment (104.5 ± 17.42 cells/mm², $p = 0.0482$) significantly reduced the density of $S100\beta^+$ astrocytes (Figure 2C and D), indicating that ciprofol also inhibits astrocyte activation. However, as shown in Figure S2A and B, no significant differences in $NeuN^+$ neuron density were observed among the groups. This suggests that the anti-inflammatory effects of ciprofol are primarily mediated by regulating glial cell activation rather than through direct effects on neurons.

To investigate the impact of ciprofol on microglial function, we assessed the expression levels of the microglial activation marker CD68—a specific indicator of microglial activation. Immunofluorescence staining revealed that the density of $CD68^+$ microglia in the PFC of CUMS model mice (163.1 ± 39.1 cells/mm²) was significantly higher than that

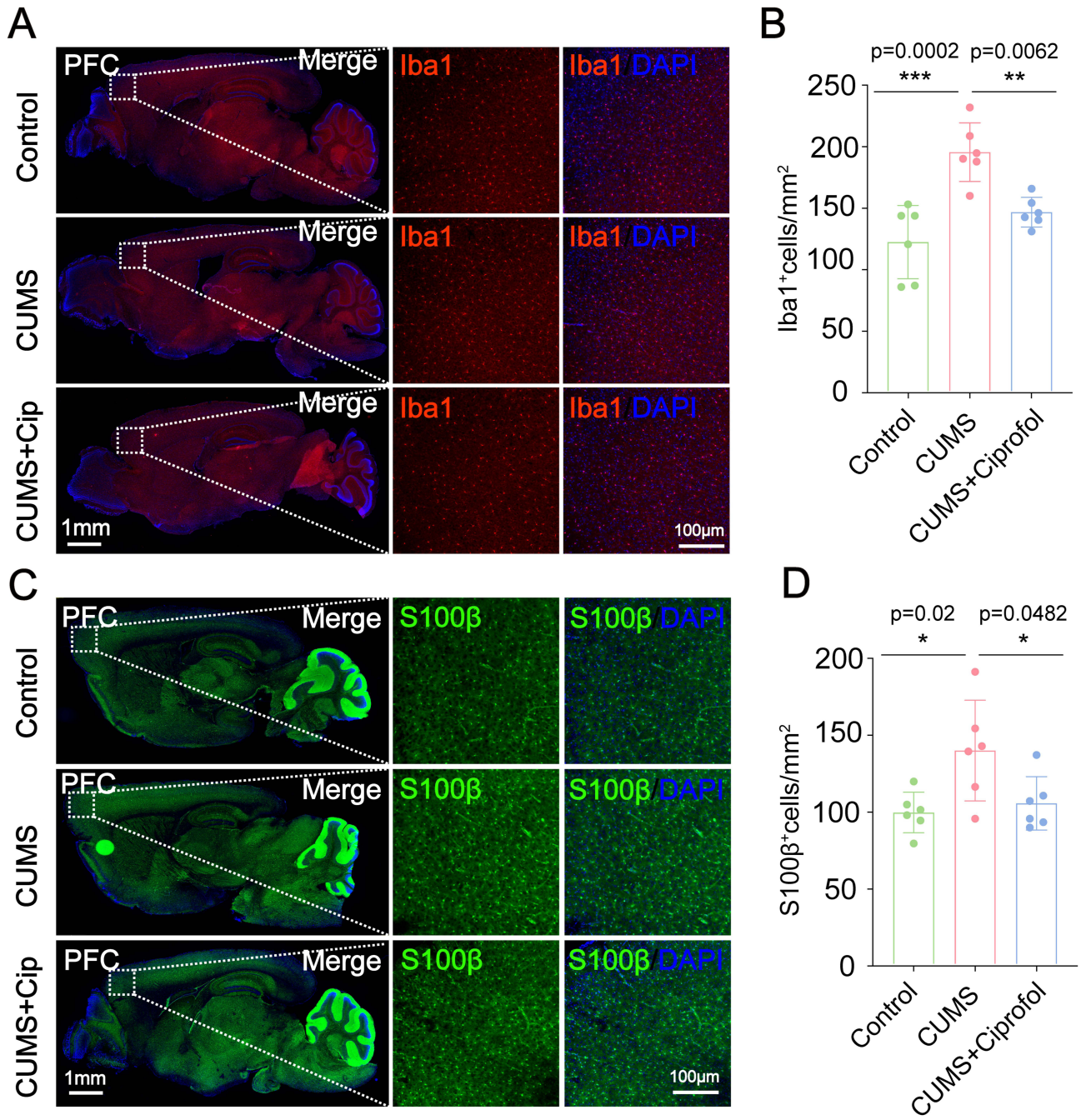

Figure 2 Ciprofol alleviates the neuroinflammation in CUMS-induced depression-like mice. (**A**) Immunostaining of Iba1 (red) in the prefrontal cortex (PFC) of the Control group, CUMS group and CUMS + Ciprofol group. (**B**) Quantification of the number of $Iba1^+$ cells per mm^2 in the PFC of the Control group, CUMS group and CUMS + Ciprofol group. (n = 6 per group, one-way ANOVA followed by Tukey's post hoc test) (**C**) Immunostaining of S100β (green) in the PFC of the Control group, CUMS group and CUMS + Ciprofol group. (**D**) Quantification of the number of $S100\beta^+$ cells per mm^2 in the PFC of the Control group, CUMS group and CUMS + Ciprofol group. (n = 6 per group, one-way ANOVA followed by Tukey's post hoc test). Images of selected regions are shown at higher magnification. All data are expressed as mean ± SD. Scale bars: 1 mm or 100 μm. *p < 0.05, **p < 0.01, ***p < 0.001.

Abbreviation: CUMS, chronic unpredictable mild stress.

in control mice (84.21 ± 23.24 cells/mm², p = 0.008), confirming that CUMS successfully induced excessive microglial activation. However, after 7 consecutive days of ciprofol treatment (98.91 ± 17.33 cells/mm², p = 0.0218), the density of $CD68^+$ microglia was significantly reduced, demonstrating that ciprofol effectively suppresses CUMS-induced microglial overactivation. (Figure 3A and B).

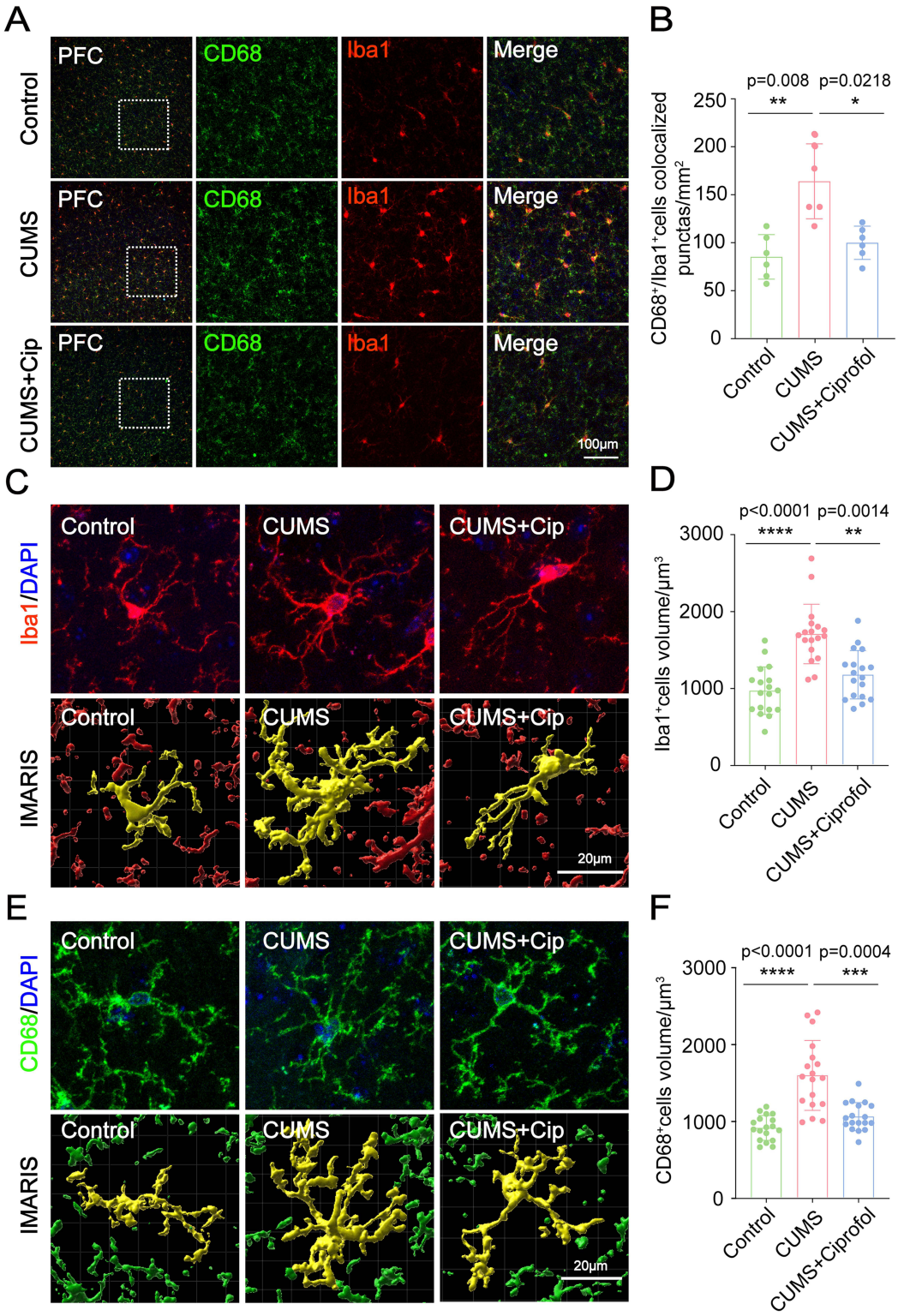

Figure 3 Ciprofol inhibits the activation of microglia in CUMS-induced depressive-like mice. (**A**) Immunostaining of CD68 (green) and Iba1 (red) in the prefrontal cortex (PFC) of the Control group, CUMS group and CUMS + Ciprofol group. (**B**) Quantification of the number of $CD68^+$ cells per mm^2 in the PFC as shown in (**A**). Images of selected regions are shown at higher magnification. (n = 6 per group, Welch's ANOVA followed by Games-Howell post hoc test) (**C**) Representative Imaris rendering of Iba1 (yellow) in the PFC of the Control group, CUMS group and CUMS + Ciprofol group. (**D**) Quantification of the volume of $Iba1^+$ microglia in the PFC region as shown in (**C**). (n = 18 cells from 6 mice per group, Kruskal–Wallis test followed by Dunn's post hoc test) (**E**) Representative Imaris rendering of CD68 (yellow) in the PFC of the Control group, CUMS group and CUMS + Ciprofol group. (**F**) Quantification of the volume of $CD68^+$ microglia in the PFC as shown in (**E**). (n = 18 cells from 6 mice per group, Welch's ANOVA followed by Games-Howell post hoc test). All data are expressed as mean ± SD. Scale bars: 20 μm or 100 μm. *p < 0.05, **p < 0.01, ***p < 0.001, ****p < 0.0001.

Abbreviation: CUMS, chronic unpredictable mild stress.

https://doi.org/10.2147/DDDT.S532905

To further elucidate the effects of ciprofol on microglial morphology and function, we used Imaris software to reconstruct three-dimensional confocal images of $CD68^+/Iba1^+$ cells. Quantitative analysis (Figure 3C–F) revealed that microglia in the PFC of CUMS model mice exhibited a typical amoeboid morphology, with the $Iba1^+$cell volume increasing by 75.7% (from 945.4 ± 306.8 μm^3 in controls to 1677 ± 383.9 μm^3, $p < 0.0001$) and the $CD68^+$ cell volume increasing by 75.5% (from 904.1 ± 161.3 μm^3 in controls to 1587 ± 454.3 μm^3, $p < 0.0001$), characteristics indicative of an overactivated state. Notably, after 7 consecutive days of ciprofol treatment, the $Iba1^+$ microglial volume was significantly reduced by 31.37% (to 1151 ± 312 μm^3 vs CUMS, $p = 0.0014$), while the $CD68^+$ microglial volume decreased by 33.8% (to 1050 ± 182.6 μm^3 vs CUMS, $p = 0.0004$). These morphological changes demonstrated a significant shift toward a resting state, indicating that ciprofol effectively reversed CUMS-induced microglial overactivation.

To comprehensively evaluate the regulatory effects of ciprofol on neuroinflammation in CUMS model mice, we performed qRT–PCR to quantify mRNA expression levels of proinflammatory cytokines in the PFC. The results showed that CUMS significantly upregulated the mRNA expression of iNOS (3.6-fold increase vs control, $p = 0.0027$), IL-6 (2.6-fold, $p = 0.008$) and IL-1β (2.9-fold, $p = 0.0103$) in the PFC (Figure S3A–C). Notably, ciprofol treatment significantly attenuated these increases (iNOS: 66.3% reduction vs CUMS, $p = 0.0046$; IL-6: 75.9%, $p = 0.0021$; IL-1β: 51.5%, $p = 0.0366$), demonstrating its potent anti-neuroinflammatory activity. To further validate these findings, we conducted in vitro experiments assessing ciprofol's regulation of proinflammatory cytokine expression. Consistent with the in vivo results, ciprofol (75 μM) significantly suppressed LPS-induced expression of TNF-α (48.6% inhibition, $p = 0.0008$) and iNOS (54.4%, $p = 0.0210$) in BV2 microglial cells (Figure S3D–E). These results collectively indicate that ciprofol exerts robust anti-inflammatory effects both in vivo and in vitro, providing mechanistic support for its ability to alleviate CUMS-induced depression-like behaviors through inhibition of neuroinflammatory pathways.

Ciprofol Inhibits the Phagocytosis of Synaptic Structures by Microglia in CUMS Model Mice

Microglial overactivation can disrupt synaptic integrity through excessive synaptic pruning. In this study, we observed enhanced microglia-mediated synaptic pruning in the PFC of CUMS mice (Figure 4A–D). Colabeling of synaptic markers vGLUT2 and PSD95 with Iba1 revealed significantly increased synaptic engulfment in CUMS mice, with vGLUT2 and PSD95 levels elevated by 299.4% ($p < 0.0001$) and 176.5% ($p = 0.0019$), respectively. These findings indicate that microglial hyperactivation promotes pathological synaptic phagocytosis, leading to synaptic structural impairment. Notably, ciprofol treatment effectively attenuated these alterations, reducing vGLUT2 levels by 30.1% ($p = 0.0482$ vs CUMS) and PSD95 by 60.9% ($p = 0.0131$). These results demonstrate that ciprofol exerts protective effects against CUMS-induced, microglia-mediated synaptic damage.

To further evaluate synaptic integrity, we performed Golgi staining to quantify dendritic spine density. The results revealed a significant reduction in dendritic spine density in CUMS model mice compared to the control group ($p = 0.0191$). Notably, ciprofol treatment substantially increased spine density by 24.8% versus the CUMS group ($p = 0.0025$; Figure 4E and F), demonstrating its ability to mitigate CUMS-induced synaptic impairment. Consistent with these morphological findings, Western blot analysis showed that ciprofol treatment significantly elevated protein expression levels of the synaptic markers PSD95 (100.4% increase vs CUMS, $p = 0.0037$) and vGLUT2 (49.5% increase vs CUMS, $p = 0.0336$; Figure 4G–I), providing molecular evidence for its protective effects on synaptic structures. These data suggest that ciprofol mitigates CUMS-induced synaptic loss, which may involve suppression of microglia-mediated pruning.

Ciprofol Exerts Antidepressant Effects Through the PPARα-Dependent ERK/CREB Signaling Pathway

To elucidate the molecular targets and mechanisms of action of ciprofol in the CUMS model, we performed transcriptome sequencing analysis on the cerebral cortex of mice from three groups: control, CUMS and CUMS + ciprofol. Compared with the control group, the CUMS group presented 388 upregulated genes and 325 downregulated genes (Figure S4A). In contrast, the CUMS + ciprofol group presented 269 upregulated genes and 261 downregulated genes

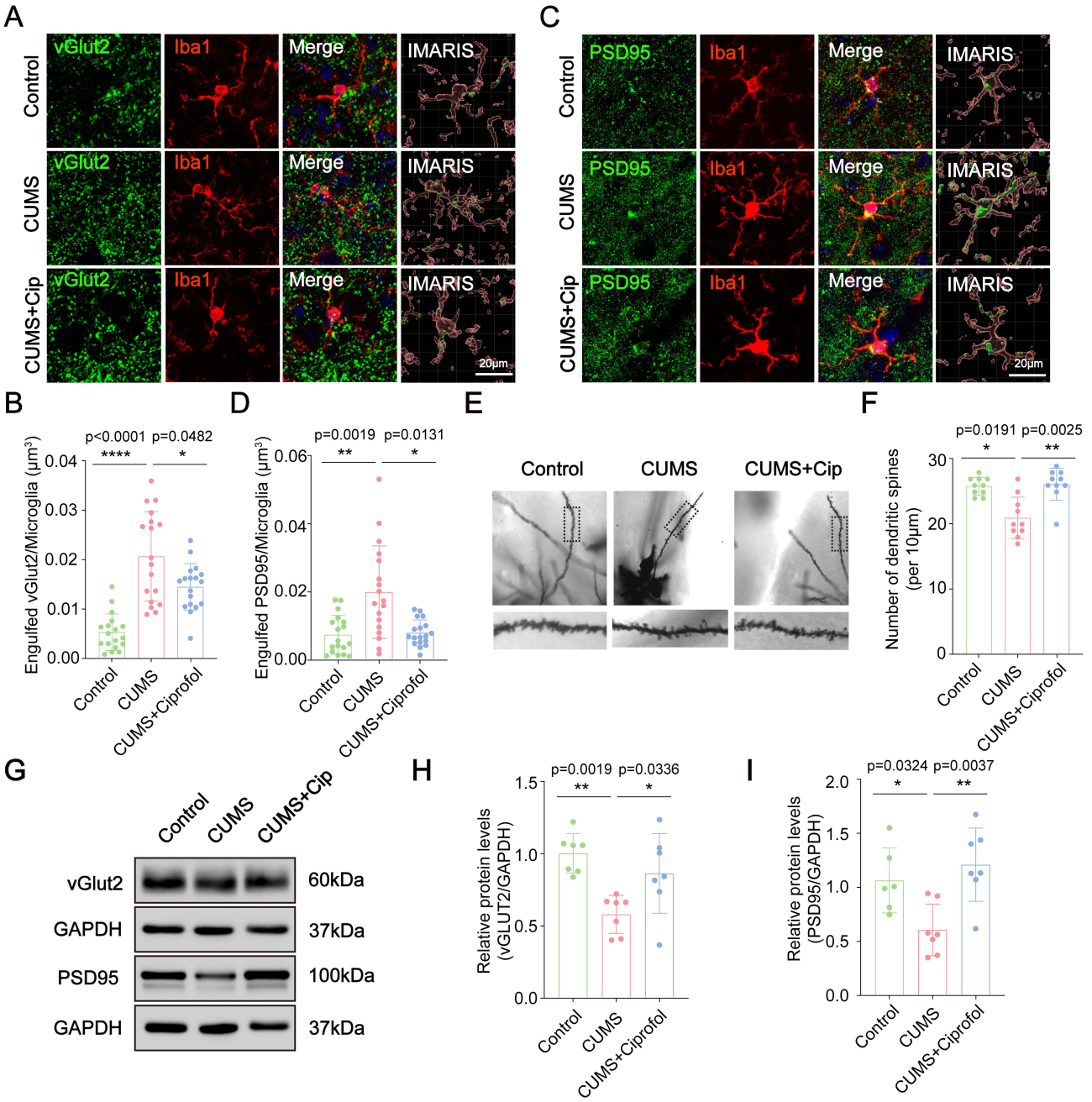

Figure 4 Ciprofol inhibits microglia-induced synaptic pruning in CUMS model mice. (**A**) Immunostaining of vGLUT2 (green) and Iba1 (red) in the prefrontal cortex (PFC) of the Control group, CUMS group and CUMS + Ciprofol group. Their merged signals and isolation of colocalized signals are also shown. (**B**) Quantification of overlapping puncta between vGLUT2 and Iba1 within Iba1$^+$ microglia, as shown in (**A**). (n = 18 from 6 mice per group, Welch's ANOVA followed by Games–Howell post hoc test) (**C**) Immunostaining of PSD95 (green) and Iba1 (red) in the PFC of the Control group, CUMS group and CUMS + Ciprofol group. Their merged signals and isolation of colocalized signals are also shown. (**D**) Quantification of overlapping puncta between PSD95 and Iba1 within Iba1$^+$ microglia, as shown in (**C**). (n = 18 from 6 mice per group, Kruskal–Wallis test followed by Dunn's post hoc test) (**E**) Imaging of the Golgi-stained dendritic spines in the PFC of the Control group, CUMS group and CUMS + Ciprofol group. (**F**) Quantification of the number of dendritic spines in PFC region as shown in (**E**). (n = 10 from 6 mice per group, Kruskal–Wallis test followed by Dunn's post hoc test) (**G**) Western blot detected the expression of vGLUT2 and PSD95 in the PFC of the Control group, CUMS group and CUMS + Ciprofol group. (**H-I**) Quantification of the relative vGLUT2 and PSD95 levels as shown in (**G**). (n = 7 mice per group, one-way ANOVA followed by Tukey's post hoc test) PSD95, postsynaptic density protein 95; vGLUT2, vesicular glutamate transporters 2. All data are expressed as mean ± SD. Scale bars: 20 μm. *p < 0.05, **p < 0.01, ****p < 0.0001.
Abbreviation:CUMS, chronic unpredictable mild stress.

compared with the CUMS group (Figure 5A). KEGG pathway analysis revealed that the DEGs between the CUMS and control groups were significantly enriched in the "ECM-receptor interaction" pathway, whereas GO analysis revealed significant enrichment in DNA binding-related terms (Figure S4B–C). These DEGs were closely associated with the

https://doi.org/10.2147/DDDT.S532905

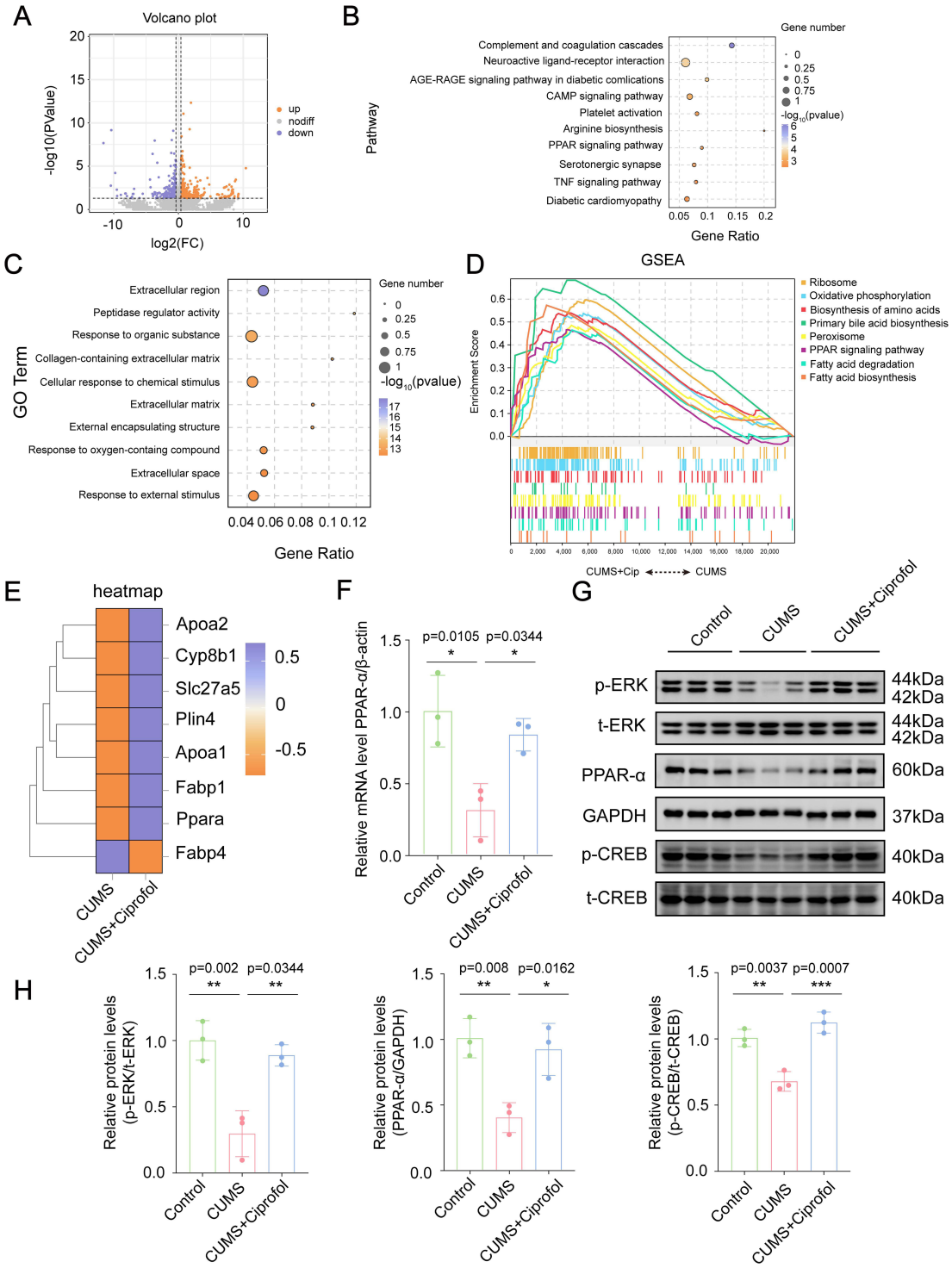

Figure 5 Identification of the potential targets and mechanisms of Ciprofol via transcriptomics. (**A**) The volcano plot showing differential expression genes between the CUMS and CUMS + Ciprofol group. Orange dots indicate up-regulated genes and purple dots indicate down-regulated genes. (**B**) The top 10 pathways of Kyoto Encyclopedia of Genes and Genomes (KEGG) enrichment analysis. (**C**) The top 10 terms of Gene Ontology (GO) analysis. (**D**) The gene set enrichment analysis (GSEA) results based on pathways terms between the CUMS and CUMS + Ciprofol group. (**E**) The heatmap involving the genes enriched in the peroxisome proliferator-activated receptor (PPAR) signaling pathway. (**F**) Quantification of the relative mRNA level of *PPARα* in the prefrontal cortex (PFC) of the Control group, CUMS group and CUMS + Ciprofol group. Data were normalized to β-actin using the $2^{-\Delta\Delta Ct}$ method and expressed as fold change relative to the Control group. (n = 3 per group, one-way ANOVA followed by Tukey's post hoc test) (**G**) Western blot detected the expression of Extracellular signal-regulated kinase (ERK), PPARα, and cAMP response element-binding protein (CREB) in the PFC of the Control group, CUMS group and CUMS + Ciprofol group. (**H**) Quantification of the relative p-ERK/ERK, PPARα and p-CREB/CREB levels as shown in (**G**). (n=3 mice per group, one-way ANOVA followed by Tukey's post hoc test) All data are expressed as mean ± SD. *p < 0.05, **p < 0.01, ***p < 0.001.

Abbreviation: CUMS, chronic unpredictable mild stress.

pathological changes induced by CUMS. Further analysis revealed that the DEGs between the CUMS + ciprofol and CUMS groups were significantly enriched in the "complement and coagulation cascades" "neuroactive ligand–receptor interaction" and "PPAR signaling pathway" (Figure 5B). Additionally, GO analysis revealed significant enrichment in terms related to "collagen-containing extracellular matrix" "cellular response to chemical stimulus" and "response to organic substance" (Figure 5C). Based on these findings, we hypothesized that the PPAR signaling pathway might be a key pathway through which ciprofol exerts its antidepressant effects. To test this hypothesis, we performed gene set enrichment analysis (GSEA) on the relevant gene sets. The results revealed significant enrichment in the "PPAR signaling pathway" as well as in metabolic regulation-related pathways such as "oxidative phosphorylation" "fatty acid degradation" and "peroxisome" (Figure S4D and Figure 5D). Heatmap analysis further revealed significant differential expression of PPAR signaling pathway-related genes (eg, Plin4, PPARα, Apoa2, Fabp1, Apoa1, Slc27a5, Cyp8b1, and Fabp4) between the CUMS and CUMS + ciprofol groups (Figure 5E). qRT–PCR confirmed that the mRNA expression level of PPARα was significantly downregulated in the CUMS group (0.3-fold vs control, $p = 0.0105$), whereas ciprofol treatment ($p = 0.0344$) significantly upregulated its expression (Figure 5F).

Additionally, our study revealed that ciprofol exerts antidepressant effects by modulating the ERK/CREB signaling pathway. Compared with those in the control group, the protein expression levels of ERK (0.3-fold, $p = 0.002$), PPARα (0.4-fold, $p = 0.008$) and CREB (0.7-fold, $p = 0.0037$) in the PFC of CUMS-induced mice were significantly lower. However, these reductions were significantly reversed following ciprofol treatment (Figure 5G and H). These data suggest that ciprofol's antidepressant effect correlates with PPARα upregulation and ERK/CREB activation, implying a possible crosstalk between these pathways.

Discussion

We systematically evaluated the antidepressant effects of ciprofol on core depressive symptoms using the SPT, TST, and FST. The results demonstrated that ciprofol exhibited distinctive dual-phase antidepressant activity in CUMS models, demonstrating rapid-onset efficacy in alleviating anhedonia within 4 h post-administration and sustained therapeutic effects on despair behaviors following 7-day treatment. Compared to propofol which only rapidly alleviates anhedonia,[14] ciprofol showed more comprehensive antidepressant effects. Ciprofol's enhanced antidepressant profile appears attributable to its optimized molecular structure, particularly the cyclopropyl modification that confers 4–5 fold greater $GABA_A$ receptor binding affinity.[18] Notably, our study found that 25 mg/kg intraperitoneal injection significantly improved depressive-like behaviors in CUMS mice, while a reported 1.6 mg/kg dose was ineffective in rat models,[42] suggesting that dosage is a critical determinant of therapeutic efficacy.

MDD is associated with GABA system dysfunction, including reduced GABA levels,[43] decreased GAD expression,[44] and impaired inhibitory neurons.[45,46] Emerging evidence suggests monoaminergic antidepressants ultimately restore glutamate-GABA balance,[47] supported by normalized GABA levels in treatment responders.[48,49] Notably, the neurosteroid allopregnanolone (Allo), a $GABA_A$ receptor modulator, reverses stress-induced HPA axis dysfunction and prevents depressive behaviors.[50] Based on these findings, we speculate that ciprofol, as a $GABA_A$ receptor agonist, exhibits dual antidepressant mechanisms: rapid anhedonia relief within 4 h via GABAergic modulation, and sustained effects through GABA restoration, neurosteroid elevation and HPA axis regulation.

Our study found that in the PFC of CUMS mice, the numbers of both microglia and astrocytes were significantly increased, which were reversed after ciprofol treatment. These findings are consistent with previous reports of astrocyte proliferation in CUMS rat models[51] but contrast sharply with observations of astrocyte atrophy and apoptosis in chronic social defeat stress (CSDS) models.[52] This discrepancy suggests that different depression models may induce distinct response patterns in glial cells.

Previous research has demonstrated that inhibiting microglia-mediated excessive synaptic pruning can significantly improve depressive-like behaviors,[53] which aligns well with our experimental results. In CUMS mice, we observed marked synaptic loss characterized by enhanced synaptic phagocytic activity of microglia, reduced dendritic spine density, and downregulation of synaptic proteins (PSD95 and vGlut2). Notably, ciprofol treatment significantly reversed these synaptic impairments. These findings support ciprofol's antidepressant effect through the regulating of microglia-synapse interactions.

Through transcriptomic and WB analyses, we observed that ciprofol treatment significantly upregulated PPARα expression at both mRNA and protein levels. As a ligand-activated transcription factor, PPARα shows developmentally

regulated expression in emotion-related brain regions including the PFC and hippocampus.[54–56] Notably, PPARα activation by its agonist PEA exhibits antidepressant effects comparable to those of fluoxetine[57] and alleviates LPS-induced depressive behaviors.[58] Our findings demonstrate that 7-day ciprofol treatment not only enhanced PPARα expression but also ameliorated depressive-like behaviors in CUMS mice. PPARα activation suppressed neuroinflammation by inhibiting glial activation,[59] reducing pro-inflammatory cytokines (TNF-α and IL-1β),[60] and downregulating NF-κB signaling.[61–63] Consistently, ciprofol decreased glial cell numbers and inflammatory markers (IL-1β, IL-6 and iNOS). Interestingly, both PPARα and ERK/CREB signaling were downregulated in CUMS mice. Previous studies suggest that PPARα agonists can rapidly induce ERK phosphorylation,[64,65] while p-ERK levels were decreased in PPARα-KO mouse models,[66] indicating a positive regulatory relationship between PPARα and ERK. Furthermore, PPARα response elements (PPREs) exist in the CREB promoter,[67] suggesting that PPARα can directly activate CREB.[68] Numerous studies have shown that activation of the ERK/CREB signaling pathway plays a crucial role in the antidepressant effects of various drugs.[69,70] We therefore propose that ciprofol exerts antidepressant effects potentially through PPARα-mediated ERK/CREB pathway activation, accompanied by reduced neuroinflammation and improved synaptic plasticity.

PPARα, a central regulator of cholesterol metabolism, may influence allopregnanolone synthesis through progesterone metabolism.[71] The PPARα agonist PEA rapidly elevates neurosteroids in emotion-related brain regions in PTSD models,[72] suggesting ciprofol's antidepressant effects may similarly involve PPARα-mediated neurosteroid regulation. Growing evidence positions PPARα as a promising target for neuropsychiatric disorders.[72–75] Notably, PPARα dysfunction in PTSD models exacerbates neuroinflammation while reducing neurosteroids.[76] Importantly, low-grade chronic inflammation has been identified as a key pathological factor increasing susceptibility to both PTSD and MDD.[77] Our findings that ciprofol upregulates PPARα and reduces inflammation suggest therapeutic potential for PTSD, particularly in cases with comorbid MDD-like symptoms.

Although this study provides valuable insights, some limitations warrant consideration. First, using only male mice prevents evaluation of potential sex differences in ciprofol's antidepressant effects, particularly given known sex-specific stress responses.[78] Second, we focused on 7-day continuous administration, leaving acute effects unexplored. Finally, clinical translation requires validation through multicenter randomized controlled trials to assess ciprofol's efficacy and safety in depressed patients.

Conclusion

Our findings demonstrate that ciprofol alleviates depressive-like behaviors in CUMS mice by suppressing neuroinflammation and preventing synaptic loss. The upregulation of PPARα expression and associated ERK/CREB signaling activation suggest a potential mechanistic basis for these therapeutic effects. These results establish ciprofol as a promising novel antidepressant candidate for further development.

Abbreviations

BSA, bovine serum albumin; CREB, cAMP response element-binding protein; CNS, central nervous system; CSDS, chronic social defeat stress; CUMS, chronic unpredictable mild stress; DAPI, 4',6-diamidino-2-phenylindole; ERK, extracellular signal-regulated kinase; FBS, fetal bovine serum; FDR, false discovery rate; FST, forced swimming test; GAPDH, glyceraldehyde-3-phosphate dehydrogenase; GABA, γ-Aminobutyric acid; GO, gene ontology; GSEA, gene set enrichment analysis; Iba1, ionized calcium-binding adapter molecule 1; IL-1β, interleukin-1β; IL-6, interleukin-6; iNOS, inducible nitric oxide synthase; KEGG, kyoto encyclopedia of genes and genomes; LPS, lipopolysaccharide; MDD, major depressive disorder; NeuN, neuronal nuclear protein; NF-κB, nuclear transcription factor-κB; PBS, phosphate-buffered saline; PFC, prefrontal cortex; PPARα, peroxisome proliferator-activated receptor α; PSD95, post synaptic density protein 95; PTSD, post-traumatic stress disorder; qRT–PCR, quantitative real-time polymerase chain reaction; SD, standard Deviation; SPT, sucrose preference test; TNF-α, tumour necrosis factor-α; TSPO, translocator protein; TRD, treatment-resistant depression; TST, tail suspension test; vGLUT2, vesicular glutamate transporters 2.

Data Sharing Statement

The data that support the study findings are available from the corresponding author upon reasonable request.

Acknowledgments

Xiuchun Li assisted with bioinformatics analysis of RNA-Seq data.

Author Contributions

All authors made a significant contribution to the work reported, whether that is in the conception, study design, execution, acquisition of data, analysis and interpretation, or in all these areas; took part in drafting, revising or critically reviewing the article; gave final approval of the version to be published; have agreed on the journal to which the article has been submitted; and agree to be accountable for all aspects of the work.

Funding

This work was supported by the National Natural Science Foundation of China (Nos.81901087 and 82271445) and the Natural Science Foundation of Zhejiang Province of China (No.LY21H090005).

Disclosure

The authors declare no conflicts of interest in this work.

References

1. Liu Q, He H, Yang J, Feng X, Zhao F, Lyu J. Changes in the global burden of depression from 1990 to 2017: findings from the global burden of disease study. *J Psychiatr Res*. 2020;126:134–140. doi:10.1016/j.jpsychires.2019.08.002
2. Beurel E, Toups M, Nemeroff CB. The bidirectional relationship of depression and inflammation: double trouble. *Neuron*. 2020;107(2):234–256. doi:10.1016/j.neuron.2020.06.002
3. Coupland C, Hill T, Morriss R, Moore M, Arthur A, Hippisley-Cox J. Antidepressant use and risk of adverse outcomes in people aged 20-64 years: cohort study using a primary care database. *BMC Med*. 2018;16(1):36. doi:10.1186/s12916-018-1022-x
4. Stahl SM. Mechanism of action of serotonin selective reuptake inhibitors. Serotonin receptors and pathways mediate therapeutic effects and side effects. *J Affect Disord*. 1998;51(3):215–235. doi:10.1016/s0165-0327(98)00221-3
5. Wyska E. Pharmacokinetic considerations for current state-of-the-art antidepressants. *Expert Opin Drug Metab Toxicol*. 2019;15(10):831–847. doi:10.1080/17425255.2019.1669560
6. Giatti S, Cioffi L, Diviccaro S, Chrostek G, Piazza R, Melcangi RC. Transcriptomic profile of the male rat hypothalamus and nucleus accumbens after paroxetine treatment and withdrawal: possible causes of sexual dysfunction. *Mol Neurobiol*. 2025;62(4):4935–4951. doi:10.1007/s12035-024-04592-9
7. Xeni F, Marangoni C, Lin L, Robinson ESJ, Jackson MG. Conditioned versus innate effort-based tasks reveal divergence in antidepressant effect on motivational state in male mice. *Neuropsychopharmacology*. 2025;doi:10.1038/s41386-025-02140-0.
8. Bozdag D, Entezari B, Gurer-Orhan H. The effects of citalopram and sertraline on adipogenesis and lipogenesis in 3T3-L1 cells. *Toxicol Lett*. 2025;405:67–75. doi:10.1016/j.toxlet.2025.02.007
9. Sepúlveda-Lizcano L, Arenas-Villamizar VV, Jaimes-Duarte EB, et al. Metabolic adverse effects of psychotropic drug therapy: a systematic review. *Eur J Investig Health Psychol Educ*. 2023;13(8):1505–1520. doi:10.3390/ejihpe13080110
10. Stimpfl JN, Walkup JT, Robb AS, et al. Deprescribing antidepressants in children and adolescents: a systematic review of discontinuation approaches, cross-titration, and withdrawal symptoms. *J Child Adolesc Psychopharmacol*. 2025;35(1):3–22. doi:10.1089/cap.2024.0099
11. Mortensen JK, Andersen G. Safety considerations for prescribing SSRI antidepressants to patients at increased cardiovascular risk. *Expert Opin Drug Saf*. 2022;21(4):467–475. doi:10.1080/14740338.2022.1986001
12. Halperin D, Reber G. Influence of antidepressants on hemostasis. *Dialogues Clin Neurosci*. 2007;9(1):47–59. doi:10.31887/DCNS.2007.9.1/dhalperin
13. Swainson J, Thomas RK, Archer S, et al. Esketamine for treatment resistant depression. *Expert Rev Neurother*. 2019;19(10):899–911. doi:10.1080/14737175.2019.1640604
14. Zhu XN, Li J, Qiu GL, et al. Propofol exerts anti-anhedonia effects via inhibiting the dopamine transporter. *Neuron*. 2023;111(10):1626–1636.e6. doi:10.1016/j.neuron.2023.02.017
15. Hausburg MA, Banton KL, Roman PE, et al. Effects of propofol on ischemia-reperfusion and traumatic brain injury. *J Crit Care*. 2020;56:281–287. doi:10.1016/j.jcrc.2019.12.021
16. Mickey BJ, White AT, Arp AM, et al. Propofol for treatment-resistant depression: a pilot study. *Int J Neuropsychopharmacol*. 2018;21(12):1079–1089. doi:10.1093/ijnp/pyy085
17. Qin L, Ren L, Wan S, et al. Design, synthesis, and evaluation of novel 2,6-disubstituted phenol derivatives as general anesthetics. *J Med Chem*. 2017;60(9):3606–3617. doi:10.1021/acs.jmedchem.7b00254
18. Jin L, Jiao CC, Chen XP, et al. The potency-ratio of ciprofol and propofol under procedural sedation and anesthesia for outpatient hysteroscopy during cervical dilation: a study using up-and-down sequential allocation method. *BMC Anesthesiol*. 2024;24(1):426. doi:10.1186/s12871-024-02793-2
19. Hu C, Ou X, Teng Y, et al. Sedation effects produced by a ciprofol initial infusion or bolus dose followed by continuous maintenance infusion in healthy subjects: a phase 1 trial. *Adv Ther*. 2021;38(11):5484–5500. doi:10.1007/s12325-021-01914-4
20. Liu Y, Yu X, Zhu D, et al. Safety and efficacy of ciprofol vs. propofol for sedation in intensive care unit patients with mechanical ventilation: a multi-center, open label, randomized, Phase 2 trial. *Chin Med J*. 2022;135(9):1043–1051. doi:10.1097/cm9.0000000000001912
21. Liu X, Ren M, Zhang A, Huang C, Wang J. Nrf2 attenuates oxidative stress to mediate the protective effect of ciprofol against cerebral ischemia-reperfusion injury. *Funct Integr Genomics*. 2023;23(4):345. doi:10.1007/s10142-023-01273-z

22. Yang Y, Xia Z, Xu C, Zhai C, Yu X, Li S. Ciprofol attenuates the isoproterenol-induced oxidative damage, inflammatory response and cardiomyocyte apoptosis. *Front Pharmacol*. 2022;13:1037151. doi:10.3389/fphar.2022.1037151
23. Dixon ML, Thiruchselvam R, Todd R, Christoff K. Emotion and the prefrontal cortex: an integrative review. *Psychol Bull*. 2017;143 (10):1033–1081. doi:10.1037/bul0000096
24. Hultman R, Mague SD, Li Q, et al. Dysregulation of prefrontal cortex-mediated slow-evolving limbic dynamics drives stress-induced emotional pathology. *Neuron*. 2016;91(2):439–452. doi:10.1016/j.neuron.2016.05.038
25. Gritti D, Delvecchio G, Ferro A, Bressi C, Brambilla P. Neuroinflammation in major depressive disorder: a review of PET imaging studies examining the 18-kDa translocator protein. *J Affect Disord*. 2021;292:642–651. doi:10.1016/j.jad.2021.06.001
26. Setiawan E, Wilson AA, Mizrahi R, et al. Role of translocator protein density, a marker of neuroinflammation, in the brain during major depressive episodes. *JAMA Psychiatry*. 2015;72(3):268–275. doi:10.1001/jamapsychiatry.2014.2427
27. Geng F, Zhao N, Ren Q. Circadian rhythm, microglia-mediated neuroinflammation, and alzheimer's disease. *Neurosci Biobehav Rev*. 2025;170:106044. doi:10.1016/j.neubiorev.2025.106044
28. Qin J, Ma Z, Chen X, Shu S. Microglia activation in central nervous system disorders: a review of recent mechanistic investigations and development efforts. *Front Neurol*. 2023;14:1103416. doi:10.3389/fneur.2023.1103416
29. Guo M, Pei WJ, Liu L, Chen K, Cheng Y, Piao XL. Neuroprotective effects of gypenosides on LPS-induced anxiety and depression-like behaviors. *Int Immunopharmacol*. 2024;143(Pt 1):113367. doi:10.1016/j.intimp.2024.113367
30. Alzarea S, Rahman S. The alpha-7 nicotinic receptor positive allosteric modulator PNU120596 attenuates lipopolysaccharide-induced depressive-like behaviors and cognitive impairment by regulating the PPAR-α signaling pathway in mice. *CNS Neurol Disord Drug Targets*. 2025;24 (3):234–244. doi:10.2174/0118715273311527240916050749
31. Liao C, Dua AN, Wojtasiewicz C, Liston C, Kwan AC. Structural neural plasticity evoked by rapid-acting antidepressant interventions. *Nat Rev Neurosci*. 2025;26(2):101–114. doi:10.1038/s41583-024-00876-0
32. Li N, Du J, Yang Y, et al. Microglial PCGF1 alleviates neuroinflammation associated depressive behavior in adolescent mice. *Mol Psychiatry*. 2025;30(3):914–926. doi:10.1038/s41380-024-02714-2
33. Yousefpour N, Tansley SN, Locke S, et al. Targeting C1q prevents microglia-mediated synaptic removal in neuropathic pain. *Nat Commun*. 2025;16 (1):4590. doi:10.1038/s41467-025-59849-1
34. Li XL, Yuan YG, Xu H, et al. Changed synaptic plasticity in neural circuits of depressive-like and escitalopram-treated rats. *Int J Neuropsychopharmacol*. 2015;18(10):pyv046. doi:10.1093/ijnp/pyv046
35. Xu F, Wu H, Xie L, et al. Epigallocatechin-3-gallate alleviates gestational stress-induced postpartum anxiety and depression-like behaviors in mice by downregulating semaphorin3A and promoting GSK3β phosphorylation in the hippocampus. *Front Mol Neurosci*. 2022;15:1109458. doi:10.3389/fnmol.2022.1109458
36. Wang YL, Wu HR, Zhang SS, et al. Catalpol ameliorates depressive-like behaviors in CUMS mice via oxidative stress-mediated NLRP3 inflammasome and neuroinflammation. *Transl Psychiatry*. 2021;11(1):353. doi:10.1038/s41398-021-01468-7
37. Xu HX, Lin SX, Gong Y, et al. Chaiyu-dixian formula exerts protective effects on ovarian follicular abnormal development in chronic unpredictable mild stress (CUMS) rat model. *Front Pharmacol*. 2020;11:245. doi:10.3389/fphar.2020.00245
38. Leng L, Zhuang K, Liu Z, et al. Menin deficiency leads to depressive-like behaviors in mice by modulating astrocyte-mediated neuroinflammation. *Neuron*. 2018;100(3):551–563.e7. doi:10.1016/j.neuron.2018.08.031
39. Chen M, Wang C, Lin Y, et al. Dorsal raphe nucleus-hippocampus serotonergic circuit underlies the depressive and cognitive impairments in 5×FAD male mice. *Transl Neurodegener*. 2024;13(1):34. doi:10.1186/s40035-024-00425-w
40. Wang G, Liu HY, Meng XW, et al. Complement C1q-mediated microglial synaptic elimination by enhancing desialylation underlies sevoflurane-induced developmental neurotoxicity. *Cell Biosci*. 2024;14(1):42. doi:10.1186/s13578-024-01223-7
41. He D, Shi X, Liang L, et al. Microglial EPOR contribute to sevoflurane-induced developmental fine motor deficits through synaptic pruning in mice. *Neurosci Bull*. 2024;40(12):1858–1874. doi:10.1007/s12264-024-01248-5
42. Yang Y, Zhou D, Min S, et al. Ciprofol ameliorates ECS-induced learning and memory impairment by modulating aerobic glycolysis in the hippocampus of depressive-like rats. *Pharmacol Biochem Behav*. 2024;239:173775. doi:10.1016/j.pbb.2024.173775
43. Hasler G, van der Veen JW, Tumonis T, Meyers N, Shen J, Drevets WC. Reduced prefrontal glutamate/glutamine and gamma-aminobutyric acid levels in major depression determined using proton magnetic resonance spectroscopy. *Arch Gen Psychiatry*. 2007;64(2):193–200. doi:10.1001/archpsyc.64.2.193
44. Karolewicz B, Maciag D, O'Dwyer G, Stockmeier CA, Feyissa AM, Rajkowska G. Reduced level of glutamic acid decarboxylase-67 kDa in the prefrontal cortex in major depression. *Int J Neuropsychopharmacol*. 2010;13(4):411–420. doi:10.1017/s1461145709990587
45. Maciag D, Hughes J, O'Dwyer G, et al. Reduced density of calbindin immunoreactive GABAergic neurons in the occipital cortex in major depression: relevance to neuroimaging studies. *Biol Psychiatry*. 2010;67(5):465–470. doi:10.1016/j.biopsych.2009.10.027
46. Fuchs T, Jefferson SJ, Hooper A, Yee PH, Maguire J, Luscher B. Disinhibition of somatostatin-positive GABAergic interneurons results in an anxiolytic and antidepressant-like brain state. *Mol Psychiatry*. 2017;22(6):920–930. doi:10.1038/mp.2016.188
47. Luscher B, Fuchs T. GABAergic control of depression-related brain states. *Adv Pharmacol*. 2015;73:97–144. doi:10.1016/bs.apha.2014.11.003
48. Sanacora G, Mason GF, Rothman DL, et al. Increased cortical GABA concentrations in depressed patients receiving ECT. *Am J Psychiatry*. 2003;160(3):577–579. doi:10.1176/appi.ajp.160.3.577
49. Sanacora G, Mason GF, Rothman DL, Krystal JH. Increased occipital cortex GABA concentrations in depressed patients after therapy with selective serotonin reuptake inhibitors. *Am J Psychiatry*. 2002;159(4):663–665. doi:10.1176/appi.ajp.159.4.663
50. Evans J, Sun Y, McGregor A, Connor B. Allopregnanolone regulates neurogenesis and depressive/anxiety-like behaviour in a social isolation rodent model of chronic stress. *Neuropharmacology*. 2012;63(8):1315–1326. doi:10.1016/j.neuropharm.2012.08.012
51. Pei Y, Liu H, Lang J, et al. rTMS ameliorates CUMS-induced anxiety-depression-like behaviour and cognitive dysfunction in rats by modulating the COX-2/PGE2 signalling pathway. *J Psychiatr Res*. 2025;186:116–128. doi:10.1016/j.jpsychires.2025.04.008
52. Shen SY, Liang LF, Shi TL, et al. Microglia-derived interleukin-6 triggers astrocyte apoptosis in the hippocampus and mediates depression-like behavior. *Adv Sci*. 2025;12(11):e2412556. doi:10.1002/advs.202412556
53. Zhao Q, Zeng C, Luo F, et al. PDE4 inhibition alleviates HMGB1/C1q/C3-mediated excessive phagocytic pruning of synapses by microglia and depressive-like behaviors in mice. *Brain Behav Immun*. 2025;126:126–143. doi:10.1016/j.bbi.2025.02.007

54. Scheggi S, Pinna G, Braccagni G, De Montis MG, Gambarana C. PPARα signaling: a candidate target in psychiatric disorder management. *Biomolecules*. 2022;12(5). doi:10.3390/biom12050723
55. Moreno S, Farioli-Vecchioli S, Cerù MP. Immunolocalization of peroxisome proliferator-activated receptors and retinoid X receptors in the adult rat CNS. *Neuroscience*. 2004;123(1):131–145. doi:10.1016/j.neuroscience.2003.08.064
56. Warden A, Truitt J, Merriman M, et al. Localization of PPAR isotypes in the adult mouse and human brain. *Sci Rep*. 2016;6:27618. doi:10.1038/srep27618
57. Yu HL, Deng XQ, Li YJ, Li YC, Quan ZS, Sun XY. N-palmitoylethanolamide, an endocannabinoid, exhibits antidepressant effects in the forced swim test and the tail suspension test in mice. *Pharmacol Rep*. 2011;63(3):834–839. doi:10.1016/s1734-1140(11)70596-5
58. Yang R, Wang P, Chen Z, et al. WY-14643, a selective agonist of peroxisome proliferator-activated receptor-α, ameliorates lipopolysaccharide-induced depressive-like behaviors by preventing neuroinflammation and oxido-nitrosative stress in mice. *Pharmacol Biochem Behav*. 2017;153:97–104. doi:10.1016/j.pbb.2016.12.010
59. Luo D, Zhang Y, Yuan X, et al. Oleoylethanolamide inhibits glial activation via moudulating PPARα and promotes motor function recovery after brain ischemia. *Pharmacol Res*. 2019;141:530–540. doi:10.1016/j.phrs.2019.01.027
60. Lama A, Pirozzi C, Severi I, et al. Palmitoylethanolamide dampens neuroinflammation and anxiety-like behavior in obese mice. *Brain Behav Immun*. 2022;102:110–123. doi:10.1016/j.bbi.2022.02.008
61. Ogawa K, Yagi T, Guo T, et al. Pemafibrate, a selective PPARα modulator, and fenofibrate suppress microglial activation through distinct PPARα and SIRT1-dependent pathways. *Biochem Biophys Res Commun*. 2020;524(2):385–391. doi:10.1016/j.bbrc.2020.01.118
62. Ramanan S, Kooshki M, Zhao W, Hsu FC, Riddle DR, Robbins ME. The PPARalpha agonist fenofibrate preserves hippocampal neurogenesis and inhibits microglial activation after whole-brain irradiation. *Int J Radiat Oncol Biol Phys*. 2009;75(3):870–877. doi:10.1016/j.ijrobp.2009.06.059
63. Ramanan S, Kooshki M, Zhao W, Hsu FC, Robbins ME. PPARalpha ligands inhibit radiation-induced microglial inflammatory responses by negatively regulating NF-kappaB and AP-1 pathways. *Free Radic Biol Med*. 2008;45(12):1695–1704. doi:10.1016/j.freeradbiomed.2008.09.002
64. Zhou Y, Chen X, Qu N, Zhang B, Xia C. Chondroprotection of PPARα activation by WY14643 via autophagy involving Akt and ERK in LPS-treated mouse chondrocytes and osteoarthritis model. *J Cell Mol Med*. 2019;23(4):2782–2793. doi:10.1111/jcmm.14184
65. Gardner OS, Dewar BJ, Earp HS, Samet JM, Graves LM. Dependence of peroxisome proliferator-activated receptor ligand-induced mitogen-activated protein kinase signaling on epidermal growth factor receptor transactivation. *J Biol Chem*. 2003;278(47):46261–46269. doi:10.1074/jbc.M307827200
66. Zhou Y, Li L, Chen X, et al. Impaired autophagy contributes to the aggravated deterioration of osteoarthritis articular cartilage by peroxisome proliferator-activated receptor α deficiency, associated with decreased ERK and Akt activation. *Eur J Med Res*. 2023;28(1):332. doi:10.1186/s40001-023-01267-4
67. Roy A, Jana M, Kundu M, et al. HMG-CoA reductase inhibitors bind to PPARα to upregulate neurotrophin expression in the brain and improve memory in mice. *Cell Metab*. 2015;22(2):253–265. doi:10.1016/j.cmet.2015.05.022
68. Bai Y, Han Q, Dong B, et al. PPARα contributes to the therapeutic effect of hydrogen gas against sepsis-associated encephalopathy with the regulation to the CREB-BDNF signaling pathway and hippocampal neuron plasticity-related gene expression. *Brain Res Bull*. 2022;184:56–67. doi:10.1016/j.brainresbull.2022.03.015
69. Yao W, Cao Q, Luo S, et al. Microglial ERK-NRBP1-CREB-BDNF signaling in sustained antidepressant actions of (R)-ketamine. *Mol Psychiatry*. 2022;27(3):1618–1629. doi:10.1038/s41380-021-01377-7
70. Chen H, Dong M, He H, et al. Ginsenoside re prevents depression-like behaviors via inhibition of inflammation, oxidative stress, and activating BDNF/TrkB/ERK/CREB signaling: an in vivo and in vitro study. *J Agric Food Chem*. 2024;72(36):19838–19851. doi:10.1021/acs.jafc.4c04394
71. Diviccaro S, Cioffi L, Falvo E, Giatti S, Melcangi RC. Allopregnanolone: an overview on its synthesis and effects. *J Neuroendocrinol*. 2022;34(2):e12996. doi:10.1111/jne.12996
72. Locci A, Pinna G. Stimulation of peroxisome proliferator-activated receptor-α by N-palmitoylethanolamine engages allopregnanolone biosynthesis to modulate emotional behavior. *Biol Psychiatry*. 2019;85(12):1036–1045. doi:10.1016/j.biopsych.2019.02.006
73. Lee Y, Cho JH, Lee S, et al. Neuroprotective effects of MHY908, a PPAR α/γ dual agonist, in a MPTP-induced Parkinson's disease model. *Brain Res*. 2019;1704:47–58. doi:10.1016/j.brainres.2018.09.036
74. Cristiano C, Pirozzi C, Coretti L, et al. Palmitoylethanolamide counteracts autistic-like behaviours in BTBR T+tf/J mice: contribution of central and peripheral mechanisms. *Brain Behav Immun*. 2018;74:166–175. doi:10.1016/j.bbi.2018.09.003
75. Deplanque D, Gelé P, Pétrault O, et al. Peroxisome proliferator-activated receptor-alpha activation as a mechanism of preventive neuroprotection induced by chronic fenofibrate treatment. *J Neurosci*. 2003;23(15):6264–6271. doi:10.1523/jneurosci.23-15-06264.2003
76. Matrisciano F, Pinna G. PPAR-α hypermethylation in the hippocampus of mice exposed to social isolation stress is associated with enhanced neuroinflammation and aggressive behavior. *Int J Mol Sci*. 2021;22(19). doi:10.3390/ijms221910678
77. Kim J, Yoon S, Lee S, et al. A double-hit of stress and low-grade inflammation on functional brain network mediates posttraumatic stress symptoms. *Nat Commun*. 2020;11(1):1898. doi:10.1038/s41467-020-15655-5
78. Salk RH, Hyde JS, Abramson LY. Gender differences in depression in representative national samples: meta-analyses of diagnoses and symptoms. *Psychol Bull*. 2017;143(8):783–822. doi:10.1037/bul0000102